MOTION COMPENSATION PROBLEM IN STRIPMAP SAS SYSTEMS

MARCIN SZCZEGIELNIAK

University of Technology and Life Sciences
Kaliskiego 7, 85-792 Bydgoszcz, Poland
marcinszczegielniak@poczta.onet.pl

Synthetic Aperture Sonar (SAS) is the high-resolution acoustic imaging technique which allows to improve the along-track resolution. A performance of SAS systems strongly depends on phase errors induced by sonar path deviations. An ideal straight path is assumed during the data gathering in such systems. The loss of coherence in the order of fraction of wavelength can result in blurring and smearing, a serious degradation of the sea-floor image. An elimination of motion errors is indispensable in order to make SAS systems applicable to high resolution imaging. Differences in motion errors modeling between systems operating in stripmap and spotlight modes are discussed. A few possible ways of the motion compensation are categorized and presented here. The results of the numerical simulation are shown and discussed in this paper.

INTRODUCTION

A stripmap SAS system in three-dimensional spatial domain (x, y, z) during the data acquisition is depicted in Figure 1A. The SAS system sends successive sound pulses perpendicular to the direction of the travel (the broadside case). In an ideal case platform's positions, at which pulses are transmitted and received, are evenly spaced. The platform position and system parameters determine the size and shape of the aperture footprint on seafloor's surface. This footprint is swept along-track as the platform moves along ping by ping illuminating the swath, so that the response of a scatterer on the seafloor is included in more than single sonar echo. An appropriate coherent combining of the signal returns (by means of a SAS reconstruction algorithm) leads to the formation of synthetically enlarged antenna, of the length 2L (Fig. 1B), what is equivalent to obtaining high-resolution reflectivity map of acoustic backscatter strength.

The assumed 'stop and hop' model (the sonar is stationary between transmitting and receiving a signal) is not particularly valid in actual conditions (especially, for SAS systems operating at long target ranges) because of the low sound speed in water. However, it was assumed in order to simplify the further analysis. To reduce this analysis to the two-dimensional spatial domain (x, r) the new variable r called slant range was defined as

$$r = \sqrt{y^2 + h^2}\ , \tag{1}$$

where h is the altitude of the platform and y denotes the spatial coordinate according to Figure 1A. The synthetic aperture domain will be represented by the variable $\boldsymbol{x'}$ in order to distinguish from the x coordinate. A signal transmitted by an antenna can be written as

$$p_{tr}(t) = p(t) \cdot \exp[i\omega_c t], \tag{2}$$

where p(t) and ω_c denote **L**inear **F**requency **M**odulated (**LFM**) signal and a carrier frequency respectively.

The influence of motion errors can be taken into account by including additional error functions $X_{err}(\boldsymbol{x'})$ and $R_{err}(\boldsymbol{x'})$ in the received signal. After receiving and demodulation of the echo signal from the scatterer located at (x,r), assuming the lossless environment, we get

$$\begin{aligned} \tilde{e}(\boldsymbol{x'},t) = \sigma \cdot p\left(t - \frac{2\sqrt{(x-\boldsymbol{x'}-X_{err}(\boldsymbol{x'}))^2 + (r-R_{err}(\boldsymbol{x'}))^2}}{c} \right) \\ \cdot \exp\left[-i\omega_c \cdot \frac{2\sqrt{(x-\boldsymbol{x'}-X_{err}(\boldsymbol{x'}))^2 + (r-R_{err}(\boldsymbol{x'}))^2}}{c} \right], \end{aligned} \tag{3}$$

where c is the sound speed in water, σ represents unknown reflectivity and $\boldsymbol{x'}$ is the position of the platform (synthetic aperture).

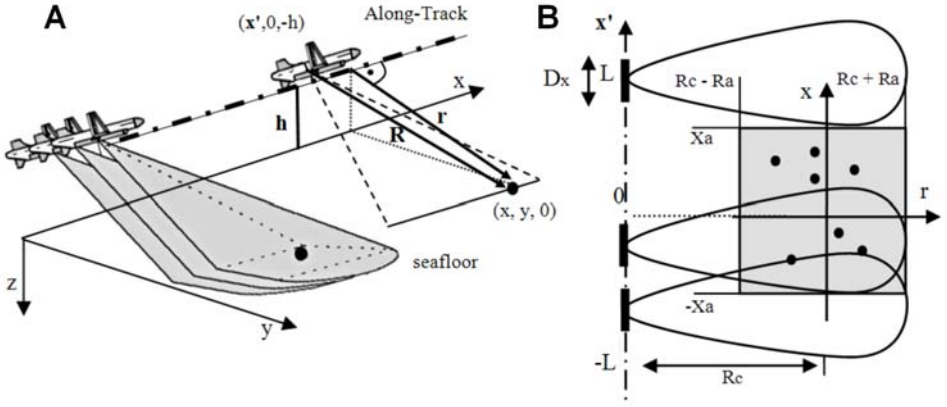

Fig.1 Synthetic aperture imaging geometry

1. MOTION ERRORS

To be precise, a towfish has six possible degrees of freedom in three-dimensional domain (x, y, z) as shown in Figure 2. However, across-track motion (sway) is the most important for side-scan SAS operation [4].

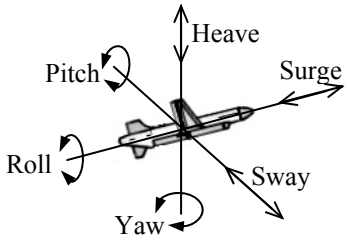

Fig.2 Sonar system motion errors

On the other hand, although sway has the most effect on SAS imagery, it is the combined effect of all six degrees of freedom on slant-range motion [5]. Mentioned above the two-dimensional mathematical model of the received SAS signal, affected by motion errors, is representation of the three-dimensional spatial domain. If a correction of motion errors in third dimension is needed the presented model can be easily extended [2].

The harmful influence of sway $R_{err}(x')$ on SAS imaging is shown in Figure 3. The sinusoidal motion error depicted in Figure 3A was injected as sway into platform's path and then the resultant image was obtained by means of the Omega-k reconstruction algorithm (Fig. 3B). For comparison, exactly the same error function as $X_{err}(x')$ doesn't cause any severe distortions in point spread function (Fig. 3C). Of course, it's possible to increase the amplitude of $X_{err}(x')$ term in order to induce blurring or smearing of the point target. However, it exceeds significantly the assumed sample spacing in the synthetic aperture domain what should not be during the data acquisition.

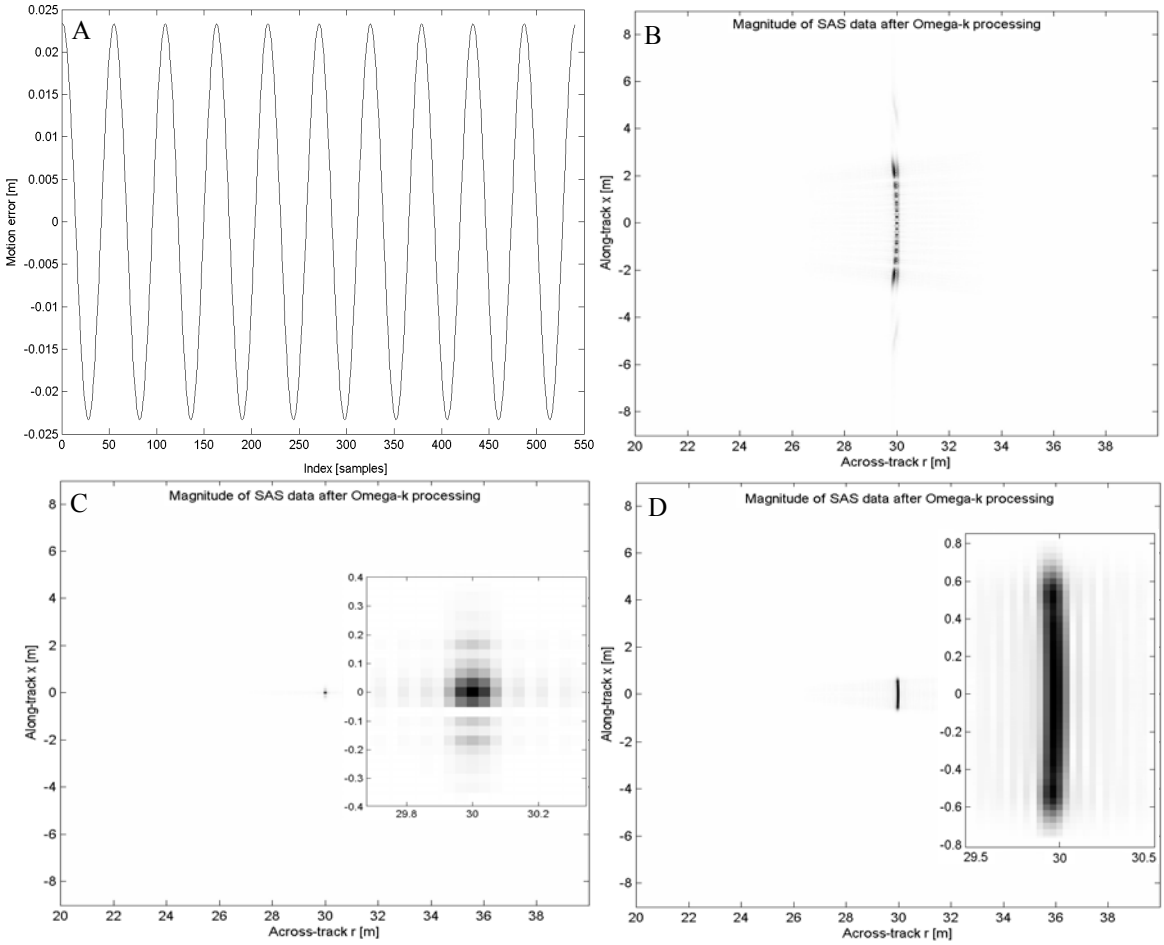

Fig.3 Results of the numerical simulation: A) motion errors; B) the reconstructed SAS image of the point target with sinusoidal motion errors injected as R_{err}; C) the reconstructed SAS image of the point target with sinusoidal motion errors injected as X_{err}; D) The reconstructed SAS image of the point target with sinusoidal motion errors of four times lower frequency than 3A (injected as R_{err})

Therefore, $X_{err}(x')$ term may be neglected in these circumstances. Slowly fluctuating motion errors are known to have a milder influence on SAS imaging, what can be seen in Figure 3D. Blur-free imagery requires $R_{err}(x') < \lambda/16$ [5] and for higher order motion errors it becomes even stricter. Sometimes, yaw compensation is applied, in particular to SAS systems

with an antenna array. Instead of performing motion compensation which suffers from the timing error approximation (described further) for each receiver independently, it is possible to remove yaw with the use of a shift and frequency scaling of wavenumber spectrum. This problem won't be analyzed here.

2. MOTION COMPENSATION APPROACHES

In general, motion compensation can be categorized according to the source of an information about motion errors [X_{err}, R_{err}]. The first category is motion compensation for known path errors thanks to a navigation unit. The second one called autofocus depends on estimating motion errors by means of only the collected SAS data. No *a priori* information is available here. The compensation for known errors can be divided into the narrow-beamwidth and wide-beamwidth in stripmap SAS systems what is discussed in the section 4. The compensation for unknown path errors contains subaperture-based techniques often called map drift, inverse filtering, Phase Gradient Autofocus (PGA) or Phase Curvature Autofocus (PCA) techniques and micronavigation. The last one relies on exploiting redundancy in the echo data. Therefore, micronavigation requires appropriate sampling rate in along-track direction in order to ensure needed redundancy. In general, the micronavigation term refers to any autofocus algorithm that operates to provide a real-time estimate of the path of the imaging platform. We can rate Redundant Phase Centre (RPC) or Shear Avarage algorithms among this group. PGA and PCA are generalization of Prominent Point Positioning (PPP) idea which will be discussed in the section 6. The basic assumption of map drift is that the aperture phase error function can be described by a finite polynomial expansion [6]. This method relies on dividing synthetic aperture into subapertures and then performing cross-correlation in order to estimate quadratic coefficients. The main its disadvantage is the impossibility of estimating higher order motion errors because of the parametric nature.

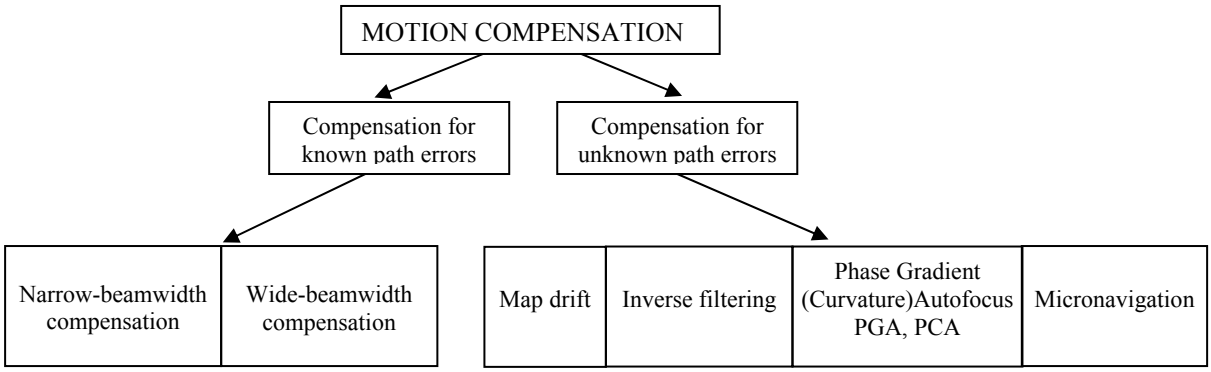

Fig.4 Conventional motion compensation approaches

3. INFLUENCE OF MOTION ERRORS ON THE RECONSTRUCTION

Let's introduce two auxiliary functions defined below

$$D_{error}(\boldsymbol{x}', x, r) = \sqrt{(x - \boldsymbol{x}' - X_{err}(\boldsymbol{x}'))^2 + (r - R_{err}(\boldsymbol{x}'))^2}\ , \tag{4}$$

$$D_{ideal}(\boldsymbol{x}', x, r) = \sqrt{(x - \boldsymbol{x}')^2 + r^2}\ , \tag{5}$$

which denote distances from the along-track position [$\boldsymbol{x}' + X_{err}(\boldsymbol{x}')$, $R_{err}(\boldsymbol{x}')$] affected by motion errors and the ideal one [$\boldsymbol{x}'$,0] to a point [x,r] respectively. The Fourier transform of the received SAS data given by (3) with respect to fast-time t can be written for the entire imaged area (x, r)

$$\tilde{e}(\boldsymbol{x}',\omega) = P(\omega)\iint_{xr} \sigma(x,r)\cdot w_a\left[\omega, x-\boldsymbol{x}'-X_{err}(\boldsymbol{x}'), r-R_{err}(\boldsymbol{x}')\right]\cdot \exp\left[-i2k\cdot D_{error}(\boldsymbol{x}',x,r)\right]dxdr \tag{6}$$

where $k=(\omega+\omega_c)/c$ is wavenumber, term $\sigma(x,r)$ describes the examined area reflectivity, P(ω) denotes the Fourier transformation of transmitted sonar signal $p(t)$ and w_a is the beam pattern of the sonar. We can rewrite equation (6) in the following way

$$\begin{aligned}\tilde{e}(\boldsymbol{x}',\omega) = P(\omega)\iint_{xr} \sigma(x,r)\cdot w_a\left[\omega, x-\boldsymbol{x}'-X_{err}(\boldsymbol{x}'), r-R_{err}(\boldsymbol{x}')\right]\cdot h(\omega, x-\boldsymbol{x}', r)\\ \cdot \exp\left[-i2k\cdot D_{ideal}(\boldsymbol{x}',x,r)\right]dxdr,\\ \text{where } h(\omega,x-\boldsymbol{x}',r)=\exp\left[i2k\cdot\Delta D(\boldsymbol{x}',x,r)\right],\\ \Delta D(\boldsymbol{x}',x,r)=D_{ideal}(\boldsymbol{x}',x,r)-D_{error}(\boldsymbol{x}',x,r).\end{aligned} \tag{7}$$

If we treat equation (7) as **AM-PM** (**A**mplitude-**M**odulated-**P**hase-**M**odulated) signal [2], where $w_a(\cdot)$ and h(·) are slowly fluctuating **AM** components in comparison with **PM** component $\exp\left[-i2k\cdot D_{ideal}(\boldsymbol{x}',x,r)\right]$, we can determine this signal in ($k_{x'}$, ω) domain using the method of stationary phase

$$\tilde{e}(k_{x'},\omega) = P(\omega)\iint_{xr} \sigma(x,r)\cdot W_a(\omega,k_{x'})\cdot H(\omega,k_{x'})\cdot \exp[-ir\cdot\sqrt{(2k)^2-(k_{x'})^2}-ix\cdot k_{x'}]dxdr, \tag{8}$$

where $H(\omega,k_{x'})$ is the simple scaling form of the term $h(\omega,x-\boldsymbol{x}',r)$ defined in the following way

$$H(\omega,2k\frac{x}{\sqrt{x^2+r^2}}) = h(\omega,x,r), \tag{9}$$

$$or \quad H(\omega,2k\sin\theta(\boldsymbol{x}')) = h(\omega,x-\boldsymbol{x}',r), \tag{10}$$

where $\theta(\boldsymbol{x}')$ is the aspect angle of the sonar for the target (x, r) when the sonar is located at $[\boldsymbol{x}'+X_{err}(\boldsymbol{x}'),\ R_{err}(\boldsymbol{x}')]$. The same relationship concerns the amplitude beam pattern $W_a(\cdot)$. The Omega-k reconstruction algorithm relies on the Stolt mapping defined below

$$k_r = \sqrt{k^2-k^2{}_{x'}}, \tag{11}$$

$$k_x = k_{x'}. \tag{12}$$

Applying Slolt mapping to (8), we get

$$\tilde{e}(k_x,k_r) = P(\omega)\iint_{xr} \sigma(x,r)\cdot W_a(\omega,k_x)\cdot H(\omega,k_x)\cdot \exp[-ir\cdot k_r - ix\cdot k_x]dxdr. \tag{13}$$

From motion compensation's point of view the most important are equations (9, 10) and (11, 12). With the aid of them we can reveal the following mapping from (k_x, k_r) to ($\boldsymbol{x}'$, ω) domain

$$H(k_r,k_x) = h(\omega,x-\boldsymbol{x}',r) = \exp\left[i2k\cdot\Delta D(\boldsymbol{x}',x,r)\right], \tag{14}$$

$$2k = \sqrt{k_r{}^2+k_x{}^2}, \tag{15}$$

$$\boldsymbol{x}' = x-\frac{k_x}{k_r}r. \tag{16}$$

To recap, an ideal SAS signal $e(k_x,k_r)$ can be related to $\tilde{e}(k_x,k_r)$ one corrupted by motion errors

$$\tilde{e}(k_x,k_r) = e(k_x,k_r)\cdot\exp\left[i\sqrt{k_r{}^2+k_x{}^2}\cdot\Delta D(x-\frac{k_x}{k_r}r,x,r)\right] \tag{17}$$

$H(k_r, k_x)$ can be considered as the spatially varying filter. The reconstructed SAS image, which should to estimate the desirable function σ(*x,r*), corrupted by motion errors is

$$\widetilde{f}(x,r) = \iint_{kx\,kr} \widetilde{e}(k_x, k_r) \cdot P^*(\omega) \exp[ik_r \cdot R_c] \cdot \exp[ik_r \cdot r + ik_x \cdot x] dk_x dk_r, \tag{18}$$

where $P^*(\omega)$ is the complex conjugate of $P(\omega)$. The additional term which has appeared in the above equations allows to bring this signal to the lowpass, i.e. this operation lets us to center the resultant SAS image at the reference distance R_c. According to Fig. 1B, R_c and X_c represent the center of the illuminated area in the cross-track and along-track domain respectively. The described case is broadside type, where $X_c=0$. If it is not, we should introduce the additional function in the form $\exp(ik_xX_c)$.

4. MOTION COMPENSATION FOR KNOWN PATH ERRORS

A navigation unit can be used to obtain an estimate of motion errors **[**$X_{err}(\boldsymbol{x}')$, $R_{err}(\boldsymbol{x}')$]. On the basis of this information, we can remove known motion errors, and thus blurring in the final SAS image. The simplest way assumes narrow beamwidth of the sonar what results in neglecting space-variant nature of the $\Delta D(\boldsymbol{x}', x, r)$ function. It's possible thanks to the following approximation

$$\Delta D(\boldsymbol{x}', x, r) \approx R_{err}(\boldsymbol{x}'). \tag{19}$$

There is no need to perform the motion compensation by spatially varying filter (according to (17)), because the approximation makes the filter $H(k_r, k_x)$ space-invariant. We can remove motion errors from pulse-compressed SAS data in ($\boldsymbol{x}'$, ω) domain by the simple operation

$$e(\boldsymbol{x}', \omega) = \widetilde{e}(\boldsymbol{x}', \omega) \cdot \exp\left[-i2kR_{err}(\boldsymbol{x}')\right]. \tag{20}$$

This solution is often called timing-error approximation. Narrow-beamwidth compensation assumes that a sideways displacement from the straight flight-path can be treated as an equivalent timing-error in the raw SAS data

$$e(\boldsymbol{x}', t) = \widetilde{e}\left(\boldsymbol{x}', t - \frac{2R_{err}(\boldsymbol{x}')}{c}\right). \tag{21}$$

For wider beamwidth this model gets less precise. If the timing-error approximation isn't acceptable we should apply wide-beamwidth model according to (17), i.e

$$e(k_x, k_r) = \widetilde{e}(k_x, k_r) \cdot H^*(k_x, k_r) \tag{22}$$

$$\text{where} \quad H^*(k_x, k_r) = \exp\left[-i\sqrt{k_r^{\,2} + k_x^{\,2}} \cdot \Delta D(x - \frac{k_x}{k_r} r, x, r)\right]$$

The filtered out single point $f(x,r)$ in the resultant motion-free SAS image is obtained by applying the filter $H^*(k_r, k_x)$ for that point and then performing inverse Fourier transform.

The problem connected with the model based on the Fourier property of **AM-PM** signals (derived in the previous section) is that the AM component ought to be slowly fluctuated one. It is highly probable that we will have to deal with higher order phase errors in practical wide-beam SAS systems. One way of mitigating this problem [2] is to perform the narrow- beamwidth compensation, and then apply the wide-beamwidth compensation with the new filter

$$H^*(k_x, k_r) = \exp\left[-i\sqrt{k_r^{\,2} + k_x^{\,2}} \cdot \Delta D_{\textbf{modified}}(x - \frac{k_x}{k_r} r, x, r)\right] \tag{23}$$

where $\Delta D_{\boldsymbol{modified}}(\boldsymbol{x}', x, r) = \Delta D(\boldsymbol{x}', x, r) - R_{err}(\boldsymbol{x}')$

Narrow-beamwitdh compensation allows to reduce the fluctuations and dynamic of the $h(\omega, x - \boldsymbol{x}', r)$ term and thus makes the derived model more accurate.

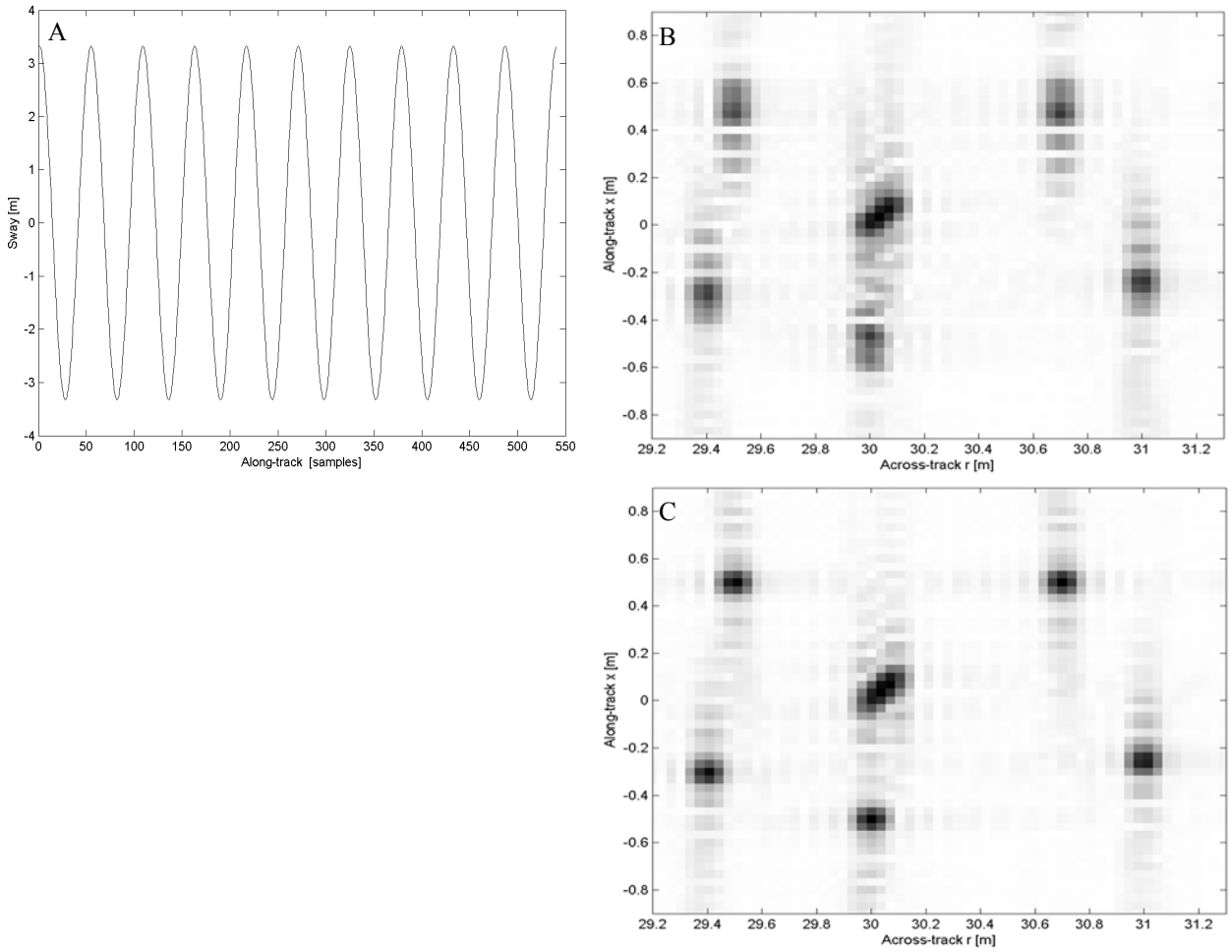

Fig.5 Results of the numerical simulation (for carrier frequency of 100 [kHz]): A) motion errors injected into the received SAS data; B) the reconstructed SAS image after narrow-beamwidth motion compensation; C) the reconstructed SAS image after narrow-beamwidth and then the modified wide-beamwidth motion compensation

5. SPOTLIGTH MODE VS STRIPMAP MODE

What makes motion compensation in stripmap SAS systems complicated (in comparison with spotlight systems) is spatially varying nature of the blurring. It's is visible in the transformation derived in the section 3, in particular, in the presence of the variable *x*.

$$\boldsymbol{x}' = x - \frac{k_x}{k_r} r. \tag{24}$$

This variable causes that each target at the coordinate *x* 'sees' the shifted error function $\Delta D(\cdot)$. Removing this term we change transformation (24) into a simple scaling. Additionally, neglecting varying character of this scaling between along-track spatial frequency and synthetic aperture position $\boldsymbol{x}'$, we get more convenient form of the transformation (24) which is suitable for spotlight systems

$$\boldsymbol{x}' = \frac{k_x}{2k_c} r, \tag{25}$$

where k_c is wavenumber at the carrier frequency. It has enormous influence on motion compensation process in spotlight mode which seems to be quite straightforward in comparison with stripmap one. Well-stated and efficient autofocus-based algorithms, commonly used in spotlight SAR systems, can't be applied to SAS stripmap systems without any modification.

6. MOTION COMPENSATION FOR UNKNOWN PATH ERRORS

Inverse filtering is the autofocus technique which is often called Prominent Point Positioning (PPP). It assumes that it's possible to remove motion errors, and thus the harmful blurring, on the basis of the information contained in the reconstructed SAS image. Let's recall the narrow-beamwidth approximation given by equation (19). Our filter can be written then in the fallowing way

$$H(k_x, k_r) \approx \exp\left[i2kR_{err}(\boldsymbol{x}')\right], \tag{26}$$

Or more general, for a squint narrow-beamwidth SAS system

$$H(k_x, k_r) \approx \exp\left[i2kR_{err}(\boldsymbol{x}')\cos\theta_S + i2kX_{err}(\boldsymbol{x}')\sin\theta_S\right], \tag{27}$$

where θ_S is the squint angle. We stated earlier that this filter can be used for motion compensation for known path errors. It's possible to estimate such the filter by means of a prominent target (x_p, r_p) in the reconstructed SAS image. What we have to do is to extract the SAS image signature $h(x - x_p, r - r_p)$ of this target. Performing the inverse Fourier transform we get

$$H(k_x, k_r) \approx \exp[i2kR_{err}(\boldsymbol{x}')]\exp[ik_x x_p + ik_r x_p]. \tag{28}$$

Next, we should remove the linear phase connected with the position of the prominent point target in the reconstructed SAS image. Otherwise, the motion correction would cause the shift of all targets. The final motion compensation is done by

$$F(k_x, k_r) \approx \widetilde{F}(k_x, k_r) \cdot H^*(k_x, k_r). \tag{29}$$

In the spotlight mode, each target should be well-focused because of the neglected term x in the equation (25). It's not so straightforward in stripmap SAS systems. The problem is that each target in the imaging scene 'sees' the shifted error function $R_{err}(\boldsymbol{x}')$ depending on its position (x, r). The received SAS signal from three point targets (C,D,E) at different locations in the scene and corrupted by sinusoidal sway (Fig. 6A) was reconstructed with the aid of Omega-k algorithm (6B). We can convince ourselves of which part of sway is 'visible' to every target. The phase of the filter $H(k_x, k_r)$ for each target signature was derived and then divided by the carrier $2k_c$ in order to obtain the estimated error function $R_{err}(\boldsymbol{x}')$ (Fig. 6C, 6D and 6E). Looking at dotted line we can note that sway for targets having different range location is not shifted. The period of 'visibility' differs only for them (compare 6C with 6D). It's strictly connected with the beamwidth of the sonar at this range (6A). It's crucial to note that the period of 'visibility' is always spread out over the entire synthetic aperture (540 samples) because of the Fourier transform of the windowed target signature. The change of the along-track location results in sway shifting as it is shown in Figures 6D and 6E.

The reconstructed SAS image (Fig. 7A) corrupted by sway (Fig. 7C) was undergone

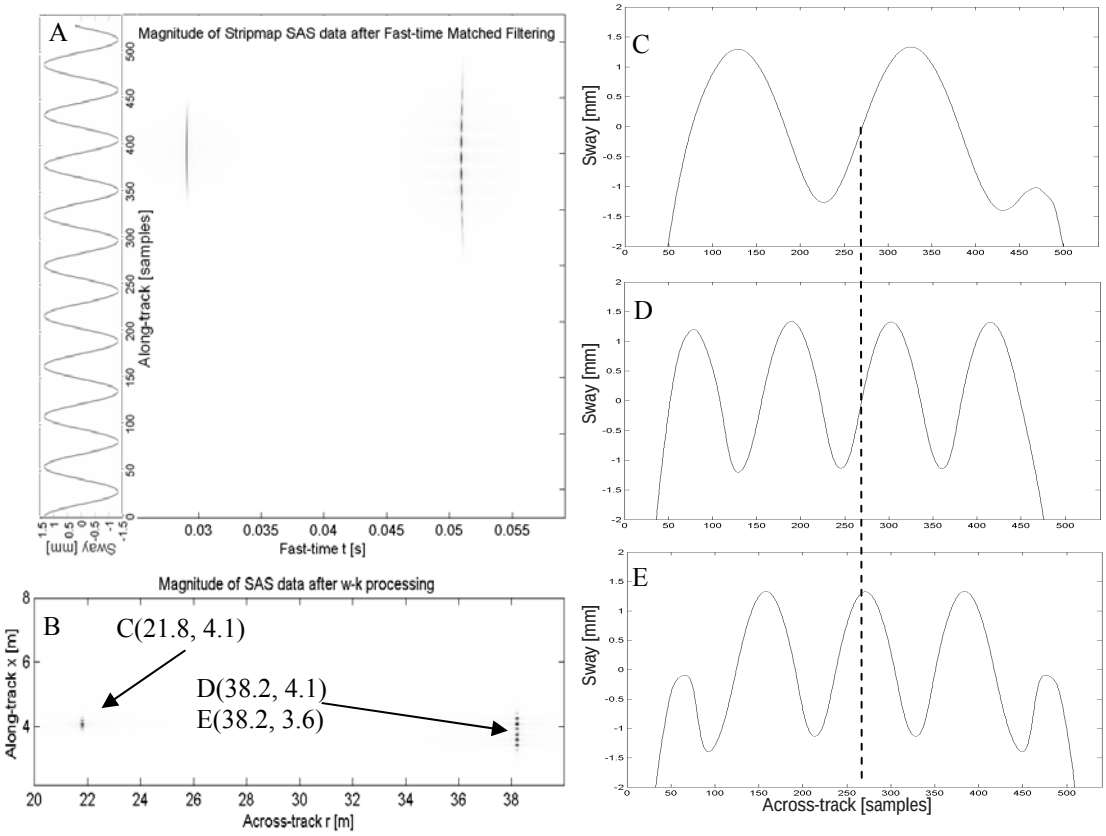

Fig.6

Fig.7 Space-variant nature of the stripmap SAS data: A) the across-track compressed SAS data with injected sway for three point targets; B) the reconstructed SAS image; C,D,E) estimated sway by means of the phase of each point target separately

inverse filtering (by means of the filter which was derived for only one prominent point. After the operation described by the equation 29) and inverse Fourier transform we get the SAS image shown in Figure 7B. We can come to the conclusion that point targets slightly distant from the prominent target in along-track direction suffer from the severe blurring. Points at the same along-track coordinate as the prominent point seem not to inherit a similar property. Therefore, one could assume range-invariant blurring and find a prominent point at every along-track line in order to remove motion errors from the entire SAS image. Unfortunately, it's not practical case in which there are not particularly many prominent targets. Moreover, these targets should be well-isolated from other surrounding targets. There are more efficient algorithms such as PCA or SPGA [5] which use take advantage of redundancy of the phase error function. However, the idea is very similar.

7. CONCLUSIONS AND REMARKS

The main goal of this paper was to outline problems connected with the motion compensation in stripmap SAS systems. The appropriate mathematical model was derived, which allowed to describe narrow-beamwidth, wide-beamwidth motion compensation, the autofocus method called inverse filtering and finally, to compare spotlight and stripmap modes in respect of motion correction. The motion compensation (narrow-beamwidth and wide-beamwidth ones) for known path errors in simulated SAS stripmap system was carried out in the Matlab environment. Results of the simulation proved the effectiveness of the two-stage compensation (compare Fig. 5B with 5C). Next, the inverse filtering method was

applied to the reconstructed and corrupted SAS image in order to reveal problems which autofocus algorithms have to cope with.

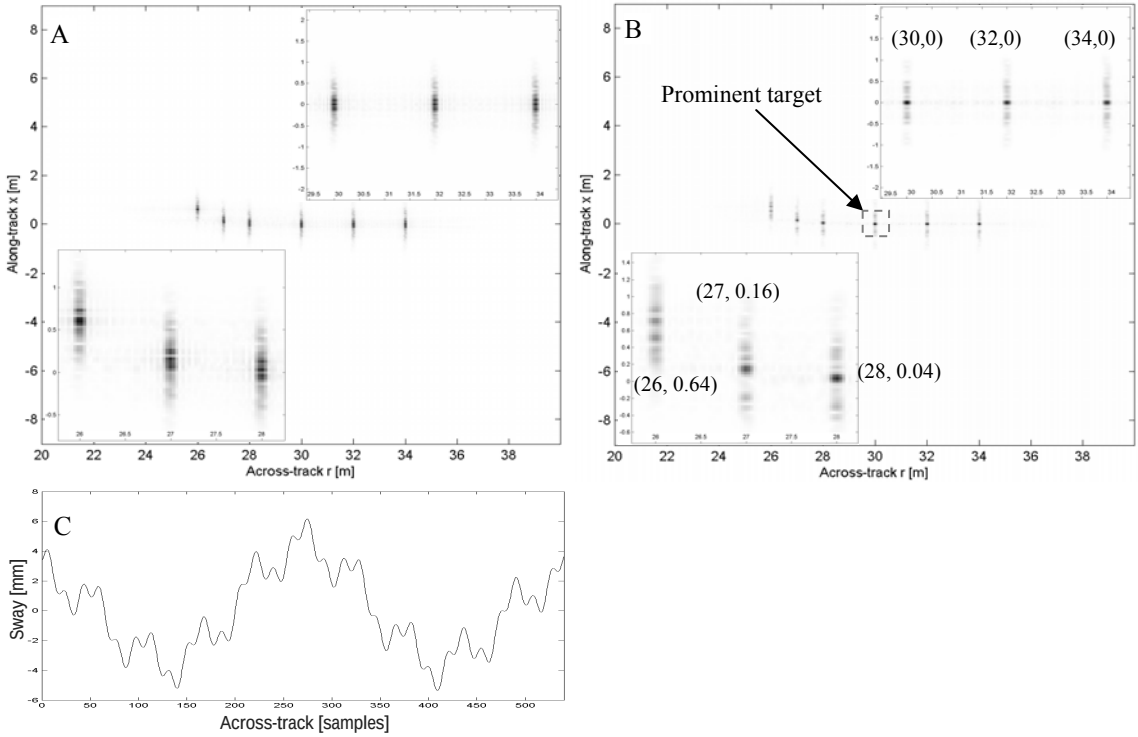

Fig.8 Results of numerical simulation (for carrier frequency of 100 [kHz]): A) the reconstructed SAS image with the presence of motion errors; B) the reconstructed SAS image after inverse filtering; C) injected sway

Robust motion compensation seems to be quite difficult task in practical stripmap SAS systems. Especially, the performance of autofocus algorithms highly depends on the imaging scene and the nature of motion errors.

REFERENCES

[1] W. Bonifant, Interferometic synthetic aperture sonar processing, MSc thesis, 38-39, Georgia Institute of Technology 1999;

[2] M. Soumekh, Synthetic aperture radar signal processing, John Wiley & Sons, 226-230, 223-226, USA 1999;

[3] M. Szczegielniak, Przetwarzanie danych SAS przy pomocy algorytmu OMEGA-K, Otwarte Seminarium z Akustyki, Poznań-Wągrowiec 2005;

[4] M.P. Hayes, P.T. Gough, Broad-band synthetic aperture sonar, IEEE Journal of Oceanic Engineering, 80-94, Jan. 1992;

[5] Hayden J. Callow, Signal processing for synthetic aperture sonar image enhancement, PhD thesis, 6,79,153 Electrical and Electronic Engineering at the University of Canterbury, New Zealand 2003;

[6] C.V. Jakowatz, D.E. Wahl, Spotlight-mode synthetic aperture radar: A signal processing approach, Springer, 245, 1996.